incorporated. Ternary hybrid nanofluids are described with mixture model [42] expressions based on the Tiwari and Das model [43]. Constant pressure gradients and viscous forces drive the flow. The Oberbeck-Boussinesq approach results in the governing equations for two-phase flow by assuming a constant pressure gradient along the channel length. Moreover, we assume that the interface has a continuous temperature, velocity, shear stress, and heat flux.

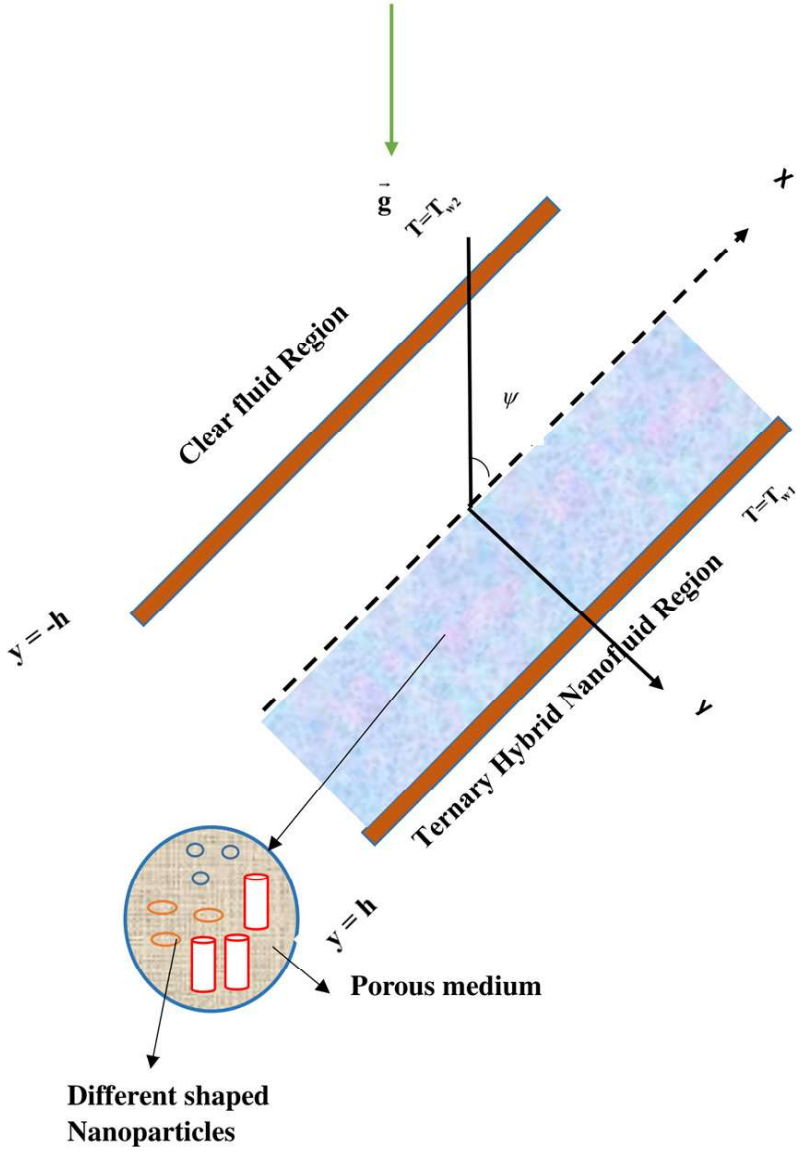

Figure 1. Flow geometry.

2.1. Governing Equations

Region-I

$$\mu_f \frac{d^2 u'_1}{dy'^2} + \left(\rho_f g \beta_f\right)(T_1 - T_{w2})\cos(\psi) - \frac{\partial p}{\partial x} = 0 \tag{1}$$

$$k_f \frac{d^2 T_1}{dy'^2} + \mu_f \left(\frac{du'_1}{dy'}\right)^2_1 - \frac{\partial q_r}{\partial y} = 0 \tag{2}$$

Region-II

$$\mu_{thnf}\frac{d^2u'_2}{dy'^2}+\left(\rho_{thnf}g\beta_{thnf}\right)(T_2-T_{w2})\cos(\psi)-\frac{\mu_{thnf}}{K}u'_2-\frac{\partial p}{\partial x}=0 \tag{3}$$

$$k_{thnf}\frac{d^2T_2}{dy'^2}+\mu_{thnf}\left(\frac{du'_2}{dy'}\right)^2+\frac{\mu_{thnf}}{K}{u'_2}^2-\frac{\partial q_r}{\partial y}=0 \tag{4}$$

Boundary and interface conditions as implemented are

$$\left.\begin{array}{l} u'_1(-h)=0, u'_1(0)=u'_2(0), \mu_f\frac{du'_1(0)}{dy'}=\mu_{thnf}\frac{du'_2(0)}{dy'},\ u'_2(h)=0 \\ T_1(-h)=T_{w2},\ T_1(0)=T_2(0),\ k_f\frac{dT_1(0)}{dy'}=k_{thnf}\frac{dT_2(0)}{dy'},\ T_2(h)=T_{w1} \end{array}\right\} \tag{5}$$

Additionally, we assessed the effect of nanoparticles with spherical, platelet, and cylindrical shapes on the base fluid's capacity to transfer heat. The thermophysical properties of nanoparticles and base fluids are calculated using a mixture model [42].

2.2. Thermophysical Properties

$$\text{Density}\quad \rho_{hnf}=(1-\phi_1-\phi_2-\phi_3)\rho_{bf}+\phi_1\rho_1+\phi_2\rho_2+\phi_3\rho_3 \tag{6}$$

Specific Heat

$$(\rho C_p)_{hnf}=(\rho C_p)_{bf}(1-\phi_1-\phi_2-\phi_3)+(\rho C_p)_1\phi_1+(\rho C_p)_2\phi_2+(\rho C_p)_3\phi_3 \tag{7}$$

Coefficient of thermal expansion

$$(\rho\beta_T)_{hnf}=(1-\phi_1-\phi_2-\phi_3)(\rho\beta_T)_{bf}+\phi_1(\rho\beta_T)_1+\phi_2(\rho\beta_T)_2+\phi_3(\rho\beta_T)_3 \tag{8}$$

Maxwell Garnett model [42]
Thermal conductivity

$$k_{nf}=k_{bf}\left(\frac{k_p+(m-1)k_f+(m-1)\phi\left(k_p-k_f\right)}{k_p+(m-1)k_f-\phi\left(k_p-k_f\right)}\right) \tag{9}$$

For spherical nanoparticles-ZrO_2

$$k_{nf1}=k_{bf}\left(\frac{k_1+(3-1)k_f+(3-1)\phi_1\left(k_1-k_f\right)}{k_1+(3-1)k_f-\phi_1\left(k_1-k_f\right)}\right) \tag{10}$$

For platelet -shaped nanoparticle-MgO

$$k_{nf2}=k_{bf}\left(\frac{k_2+4.7k_f+4.7\phi_2\left(k_2-k_f\right)}{k_2+4.7k_f-\phi_2\left(k_2-k_f\right)}\right) \tag{11}$$

For cylindrical-shaped nanoparticle-SWCNT

$$k_{nf3}=k_{bf}\left(\frac{k_3+3.9k_f+3.9\phi_3\left(k_3-k_f\right)}{k_3+3.9k_f-\phi_3\left(k_3-k_f\right)}\right) \tag{12}$$

Viscosity in terms of the Einstein–Batchelor equation [44,45]
For spherical nanoparticles -ZrO_2

$$\mu_{nf1}=\mu_f\left(1+2.5\phi_1+6.2\phi_1^2\right) \tag{13}$$

For platelet-shaped nanoparticle-MgO

$$\mu_{nf2} = \mu_f\left(1 + 37.1\phi_2 + 612.6\phi_2^2\right) \tag{14}$$

For cylindrical-shaped nanoparticle-SWCNT

$$\mu_{nf3} = \mu_f\left(1 + 13.5\phi_3 + 904.4\phi_3^2\right) \tag{15}$$

Dynamic viscosity of ternary hybrid nanofluid.

$$\mu_{hnf} = \mu_{nf1} \times \phi_1 + \mu_{nf2} \times \phi_2 + \mu_{nf3} \times \phi_3 \tag{16}$$

Effective thermal conductivity of ternary hybrid nanofluid

$$k_{hnf} = \frac{k_{nf1}\phi_1 + k_{nf2}\phi_2 + k_{nf3}\phi_3}{\phi_{hnf}} \tag{17}$$

where $\phi_{hnf} = \phi_1 + \phi_2 + \phi_3$.

Rosseland's estimate [46] provides the formula for the radiant heat flux [47] in the direction of y'

$$q_r = -\frac{4\sigma_s}{3k_a}\frac{\partial}{\partial y'}\left(T^4\right) \tag{18}$$

The scope of the current analysis is restricted to optically thick fluids as a result of the Rosseland approximation's application. If the temperature changes within the flow are modest enough, expanding T^4 into the Taylor series about T_∞ while ignoring higher-order variables allows us to construct a linear form of Equation (13) as shown below.

$$T^4 = 4\left(T_\infty^3 T\right) - 3T_\infty^4 \tag{19}$$

Further, the term $\frac{\partial q_r}{\partial y'}$ in (2) and (4) will become

$$\frac{\partial q_r}{\partial y'} = -\frac{16}{3}\left(\frac{\sigma_s T_\infty^3}{k_a}\right)\frac{\partial^2 T}{\partial y'^2} \tag{20}$$

Since ternary hybrid nanofluid is composed of spherical, platelet-shaped, and cylindrical nanoparticles, Table 2 displays the relevant sphericity and shape parameters.

Table 2. Values of sphericity and shape factor [39].

Shape	Spherical	Platelets	Cylindrical
Sphericity (η)	1	0.52	0.612
Shape factor (m)	3	5.7	4.9

2.3. Non-Dimensional Parameters for Region-I and II

$$y = \frac{y'}{h},\ u_i = u'_i\left(\frac{\rho_f}{\mu_f}\right)h,\ \theta_i = \frac{T_i - T_{w2}}{T_{w1} - T_{w2}},\ G_{r1} = \frac{g\beta_f(T_{w1} - T_{w2})h^3}{v_f^2},$$

$$Grt = G_{r1}\mathrm{Cos}(\gamma),\ Br = \frac{\mu_f^3}{\rho_f^2 h^2(T_{w1} - T_{w2})k_f}\sigma = \frac{h}{\sqrt{K}},\ P = -\frac{\rho_f h^3}{\mu_f^2}\frac{\partial p}{\partial x},$$

$$v_f = \frac{\mu_f}{\rho_f},\ R = \frac{16\sigma_s T_\infty^3}{3K_a k_f} \tag{21}$$

Upon substituting above-mentioned dimensionless parameters into Equations (1)–(5), we get

Region-I

$$\frac{d^2u_1}{d^2y} + (Grt\theta_1) + P = 0 \tag{22}$$

$$N_1\frac{d^2\theta_1}{dy^2} + Br\left\{\left(\frac{du_1}{dy}\right)^2\right\} = 0 \tag{23}$$

Region-II

$$\frac{d^2u_2}{dy^2} + aGrt\theta_2 - \sigma^2u_2 + P_1 = 0 \tag{24}$$

$$N_2\frac{d^2\theta_2}{dy^2} + Brc\left[\left(\frac{du_2}{dy}\right)^2 + \sigma^2u_2^2\right] = 0 \tag{25}$$

For Region-I and Region-II, these are the boundary and interface conditions:

$$\begin{array}{lll} At & y=-1 & \left.\begin{array}{c} u_1=0 \\ \theta_1=0 \end{array}\right\} \\ At & y=0 & \left.\begin{array}{c} u_1=u_2 \\ \theta_1=\theta_2 \end{array}\right\} \\ At & y=0 & \left.\begin{array}{c} \frac{du_1}{dy}=\frac{\mu_{thnf}}{\mu_f}\frac{du_2}{dy} \\ \frac{d\theta_1}{dy}=\frac{k_{thnf}}{k_f}\frac{d\theta_2}{dy} \end{array}\right\} \\ At & y=1 & \left.\begin{array}{c} u_2=0 \\ \theta_2=1 \end{array}\right\} \end{array} \tag{26}$$

3. Method of Solution

The nature of the transport Equations (22)–(26) are non-linear where exact analytical solutions are not possible. Therefore, by employing the Regular perturbation technique, the approximate solution for temperature and velocity is obtained. The perturbation parameter considered here is the Brinkmann number.

$$\left.\begin{array}{c} u_i = u_{i0} + Bru_{i1} + Br^2u_{i2} + \ldots \\ \theta_i = \theta_{i0} + Br\theta_{i1} + Br^2\theta_{i2} + \ldots \end{array}\right\} \tag{27}$$

Upon substituting (22)–(26) in (27) and equating equal powers of the Brinkmann number to zero, we get following equations.

Region-I

Zeroth order

$$\frac{d^2u_{10}}{dy^2} + (Grt\theta_{10}) + P = 0 \tag{28}$$

$$\frac{d^2\theta_{10}}{dy^2} = 0 \tag{29}$$

First order

$$\frac{d^2u_{11}}{d^2y} + (aGrt\theta_{11}) = 0 \tag{30}$$

$$N_1\frac{d^2\theta_{11}}{dy^2} + \left\{\left(\frac{du_{10}}{dy}\right)^2\right\} = 0 \tag{31}$$

Region-II

Zeroth order

$$\frac{d^2u_{20}}{dy^2} + aGrt\theta_{20} - \sigma^2u_{20} + P_1 = 0 \tag{32}$$

$$\frac{d^2\theta_{20}}{dy^2} = 0 \tag{33}$$

First order

$$\frac{d^2u_{21}}{dy^2} + aGrt\theta_{21} - \sigma^2 u_{21} = 0 \tag{34}$$

$$N_2\frac{d^2\theta_{21}}{dy^2} + c\left[\left(\frac{du_{20}}{dy}\right)^2 + \sigma^2 u_{20}^2\right] = 0 \tag{35}$$

For the zeroth and first order, conditions at the boundary and interface are

$$\left.\begin{array}{c} u_{10}(-1) = 0, u_{10}(0) = u_{20}, \mu_f \frac{du_{10}}{dy}(0) = \mu_{thnf}\frac{du_{20}}{dy}(0), u_{20}(1) = 0 \\ \theta_{10}(-1) = 0, \theta_{10}(0) = \theta_{20}(0), k_f \frac{d\theta_{10}}{dy}(0) = k_{thnf}\frac{d\theta_{20}}{dy}(0), \theta_{20}(1) = 1 \end{array}\right\} \tag{36}$$

$$\left.\begin{array}{c} u_{11}(-1) = 0, u_{11}(0) = u_{21}(0), \mu_f \frac{du_{11}}{dy}(0) = \mu_{thnf}\frac{du_{21}}{dy}(0), u_{21}(1) = 0 \\ \theta_{11}(-1) = 0, \theta_{11}(0) = \theta_{21}(0), k_f \frac{d\theta_{11}}{dy}(0) = k_{thnf}\frac{d\theta_{21}}{dy}(0), \theta_{21}(1) = 1 \end{array}\right\} \tag{37}$$

where, u_i, θ_i $(i = 1, 2)$ are functions of y.

The zeroth and first order solutions for the distributions of temperature and velocity are

Temperature distribution

$$\theta_{10} = b_1 y + b_2 \tag{38}$$

$$\theta_{20} = b_3 y + b_4 \tag{39}$$

$$\theta_{11} = -\frac{1}{N_1}\left(L_5 y^6 + L_6 y^5 + L_7 y^4 + L_8 y^3 + L_9 y^2\right) + c_{31} y + c_{32} \tag{40}$$

$$\theta_{21} = \frac{-c}{N_2}\left(\begin{array}{c} L_{20}\cosh 2\sigma y + L_{21}\sinh 2\sigma y + L_{22} y\cosh\sigma y + L_{23} y\sinh\sigma y \\ +L_{24}\cosh\sigma y + L_{25}\sinh\sigma y + L_{26}y^4 + L_{27}y^3 + L_{28}y^2 \end{array}\right) + c_{41} y + c_{42} \tag{41}$$

Velocity distribution

$$u_{10} = L_1 y^3 + L_2 y^2 + c_{11} y + c_{12} \tag{42}$$

$$u_{20} = c_{21}\cosh\sigma y + c_{22}\sinh\sigma y - \frac{1}{\sigma^2}(L_3 y + L_4) \tag{43}$$

$$u_{11} = \frac{aGr}{N_1}\left(L_{37}y^8 + L_{38}y^7 + L_{39}y^6 + L_{40}y^5 + L_{41}y^4 + L_{42}y^3 + L_{43}y^2\right) + c_{51} y + c_{52} \tag{44}$$

$$u_{21} = -aGrt\left(\begin{array}{l} c_{61}\cosh\sigma y + c_{62}\sinh\sigma y + L_{29}\cosh 2\sigma y \\ +L_{30}\sinh 2\sigma y + L_{31}y^2\sinh\sigma y - L_{32} y\cosh\sigma y + L_{33}y^2 cosh\sigma y \\ +L_{34} y\sinh\sigma y + L_{35}\sinh\sigma y + L_{36} y\cosh\sigma y \\ -\frac{1}{\sigma^2}\left(L_{26}y^4 + L_{27}y^3 + L_{28}y^2 + \frac{1}{\sigma^2}\left(12L_{26}y^2 + 6L_{27}y + 2L_{28}\right)\right) - \frac{1}{\sigma^2}(c_{31}y + c_{32}) \end{array}\right) \tag{45}$$

where $b_1, b_2, b_3, b_4, L_1, L_2, \ldots . L_{43}$ are constants given in the Appendix A, and $c_{11}, c_{12}, c_{21}, c_{22}, c_{31}, c_{32}, c_{41}, c_{42}, c_{51}, c_{52}, c_{61}, c_{62}$ are the constants obtained during integration.

Consequently, the result of the temperature and velocity equation will be

$$\left.\begin{array}{l} \theta_1 = \theta_{10} + Br\theta_{11} \\ \theta_2 = \theta_{20} + Br\theta_{21} \end{array}\right\} \tag{46}$$

$$\left.\begin{array}{l} u_1 = u_{10} + Bru_{11} \\ u_2 = u_{20} + Bru_{21} \end{array}\right\} \tag{47}$$

where, u_i, $\theta_i (i = 1, 2)$ are functions of y.

Physical Quantities

The non-dimensional derived quantities are determined as follows due to engineering understanding.

Nusselt Number:

$$(Nu_1) = \left(\frac{d\theta_1}{dy}\right)_{y=-1}, \ (Nu_2) = \left(\frac{d\theta_2}{dy}\right)_{y=1} \tag{48}$$

Skin Friction coefficient:

$$(Sk_1) = \left(\frac{du_1}{dy}\right)_{y=-1}, \ (Sk_2) = \left(\frac{du_2}{dy}\right)_{y=1} \tag{49}$$

Further,

The dimensionless total volume flow rate can be calculated using

$$Q_{Vol} = Q_{Vol1} + Q_{Vol2} \tag{50}$$

where $Q_{Vol1} = \int_{-1}^{0} u_1 dy$, $Q_{Vol2} = \int_{0}^{1} u_2 dy$.

The dimensionless total heat rate added to the flow is calculated using

$$E = \int_{-1}^{0} u_1\theta_1 dy + \int_{0}^{1} u_2\theta_2 dy \tag{51}$$

4. Results and Discussions

In-depth discussion of ternary hybrid nanofluids' relevance and potential applicability to practical issues is provided in this article. The interaction between three differently shaped nanoparticles and PEG water is examined in this work. We have blended the PEG water with a combination of spherical ZrO_2, platelet-shaped MgO, and SWCNT. In order to completely comprehend the flow model, the solution of temperature and velocity is obtained using the regular perturbation method. Tables and graphs are used to display the data. The thermal Grashof number ($1 \leq Gr \leq 15$), the Brinkman number ($0 \leq Br \leq 1$), the radiation parameter, the porosity parameter ($2 \leq \sigma \leq 8$), and the ϕ_1, ϕ_2, ϕ_3 are the nanoparticle volume fractions of ZrO_2, MgO, and SWCNT, respectively, and were used as non-dimensionalized constraints to supervise the flow. The following values of the non-dimensional parameters are considered for graphs and tables except the varying parameter. In this context, clear fluid denotes PEG–water, ternary hybrid nanofluid denotes PEG–Water + MgO + ZrO_2, and $y = -1$ and $y = 1$ denote the upper and bottom plates, respectively.

$$Grt = 5,\ P = 5,\ \sigma = 4,\ \phi_1 = \phi_2 = \phi_3 = 0.02,\ Br = 0.5, \psi = \pi/6,\ R = 0.6$$

The thermal Grashof number greatly impacts both the temperature and velocity fields, as shown in Figure 2. As *Grt* increases, the temperature of the fluid rises in both regions. However, temperature enhancement is primarily substantial in the ternary nanofluid region. Although viscosity forces work against natural convection, they become less powerful as *Grt* increases. Natural convection will therefore start when the *Grt* is big enough since the buoyancy forces will be stronger than the viscosity forces. As a result, the fluid's temperature increases. The second region is also filled with a ternary hybrid nanofluid, which has a higher thermal conductivity than clear fluid. The ternary hybrid nanofluid area consequently exhibits the highest enhancement. The impact of on the velocity field is shown in Figure 2. While *Grt* in this case exhibits behaviour akin to that of temperature, it is discovered that velocity is greatest in the region of clear fluid. Because hybrid ternary nanofluid has a high density, it resists flow. As a result, the velocity in the area of clear fluid rises. The results attained are identical to those of Malashetty et al. [48]. The efficiency of the system as a whole can be increased by incorporating natural convection and heat transfer into solar collectors or heat storage devices.

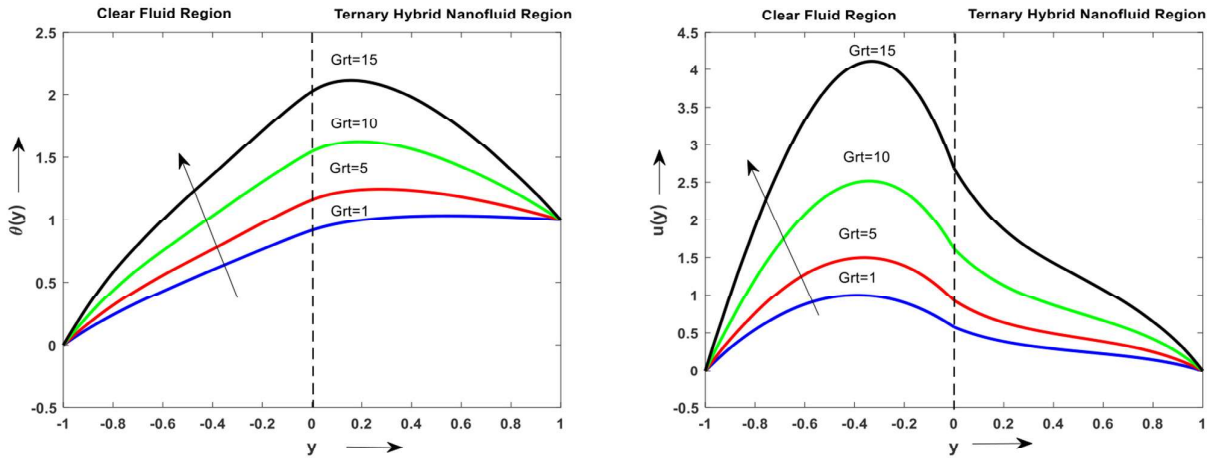

Figure 2. The impact of Grt on $\theta(y)$ and $u(y)$.

As seen in Figure 3, porous media have an impact on temperature and velocity profiles. As σ increases, both regions experience a sudden drop in temperature and fluid velocity. Additionally, the lowering effect has a greater impact in the clear fluid zone for the temperature profile as compared to the ternary nanofluid region. Additionally, the ternary nanofluid zone exhibits a greater reduction in fluid velocity. Complex flow patterns may result from the interaction of the fluid with the porous material. Porous media are frequently used in the oil and gas sector. Optimum oil recovery may be achieved by using porous media with reasonable porosity values, understanding fluid flow, and heat transfer. Similar results have been observed with Umavathi and Hemavathi [49] for all three regions.

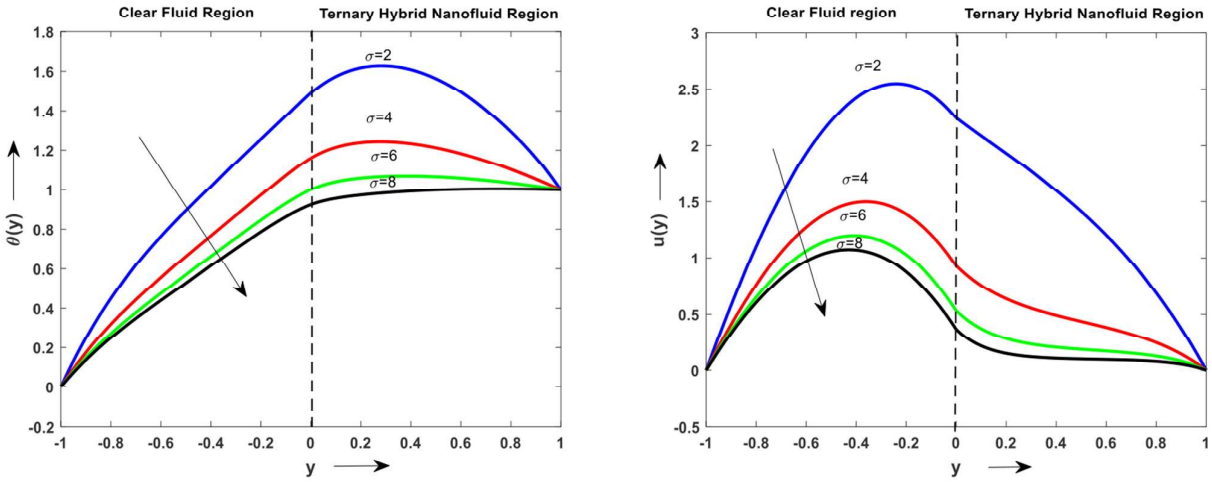

Figure 3. The impact of σ on $\theta(y)$ and $u(y)$.

The impact of Br on temperature and velocity can be viewed in Figure 4. The fluid's temperature rises as Br's value increases. The ternary hybrid nanofluid region exhibits the greatest temperature increase. The capacity of the fluid to transfer heat slows down as Br rises, which enhances the heat generated via viscous dissipation. As a result, the fluid's temperature increases. Furthermore, the impact of Br on the velocity profiles is also shown in Figure 4. In contrast to the ternary hybrid nanofluid region, the clear fluid region has a higher velocity. As Br increases, the viscous dissipation overrides the external heat by conduction. Thus, some kinetic energy in the fluid is converted into thermal energy by its viscosity, which in turn results in an increase in velocity.

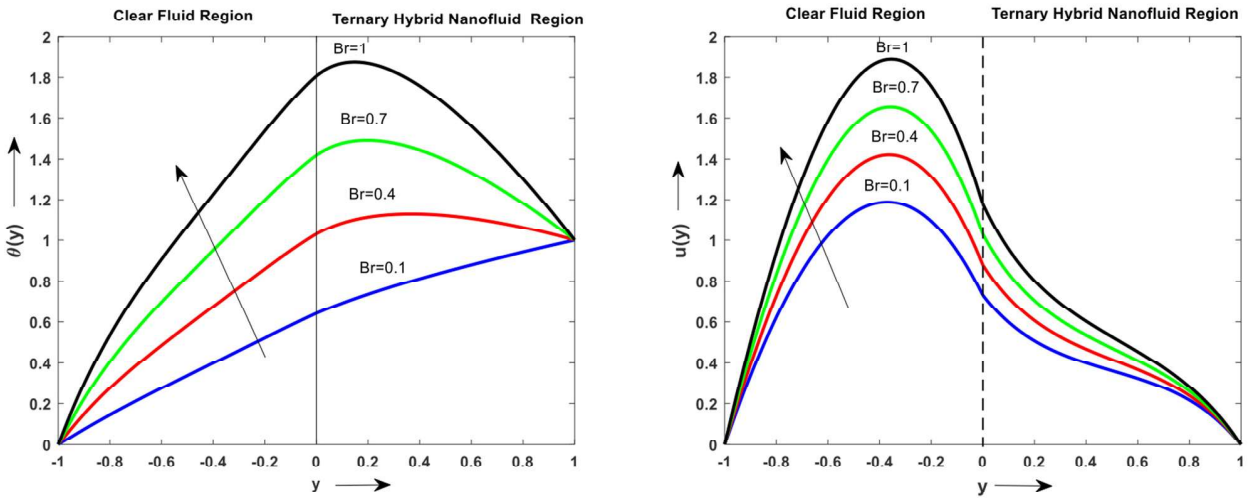

Figure 4. The impact of Br on $\theta(y)$ and $u(y)$.

The consequence of R on temperature and velocity profiles is shown in Figure 5. Increasing R results in a decreasing fluid temperature, as seen in Figure 5. The fluid's temperature is anticipated to drop as radiation slows the rate of energy transfer into the fluid. A similar phenomenon is observed for the velocity profiles depicted in Figure 5. In contrast to the previous observation, the velocity in the region of the ternary nanofluid decreased. The results are in accordance with those of Das et al. [50].

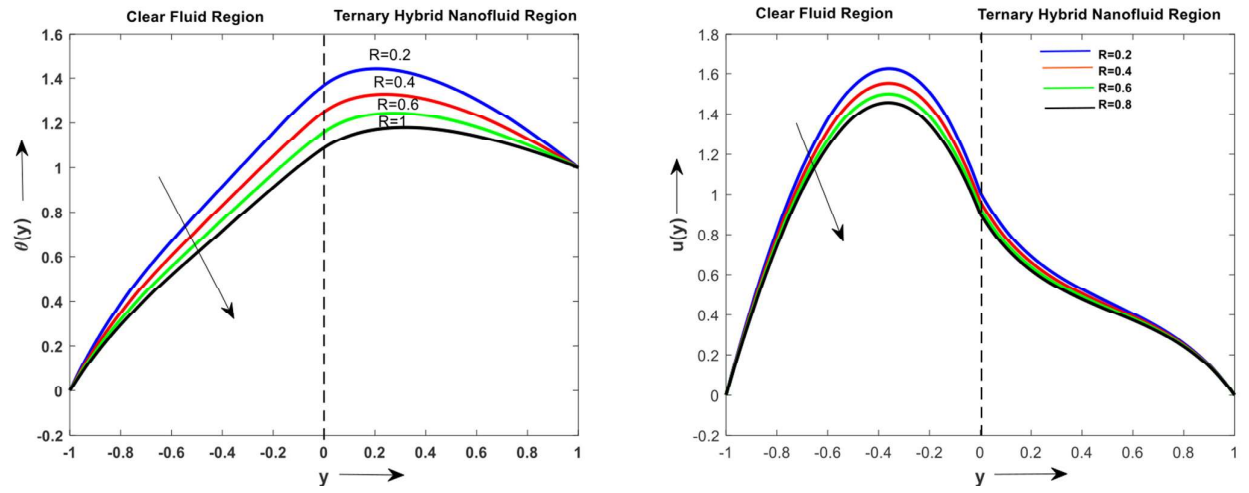

Figure 5. The impact of R on $\theta(y)$ and $u(y)$.

The temperature and velocity profiles are affected by the volume fraction of ZrO_2, as seen in Figure 6. The value of ϕ_1 is varied by considering ϕ_2 and ϕ_3 as constants. Figure 6 makes clear that as ϕ_1 is increased, the fluid's temperature increases. As particle concentrations increase, the fluid's resistive forces also grow, which amplifies kinetic energy and raises the fluid's temperature. The velocity profiles illustrated in Figure 6 exhibit a similar effect. But the velocity of the fluid is relatively high in the clear fluid region.

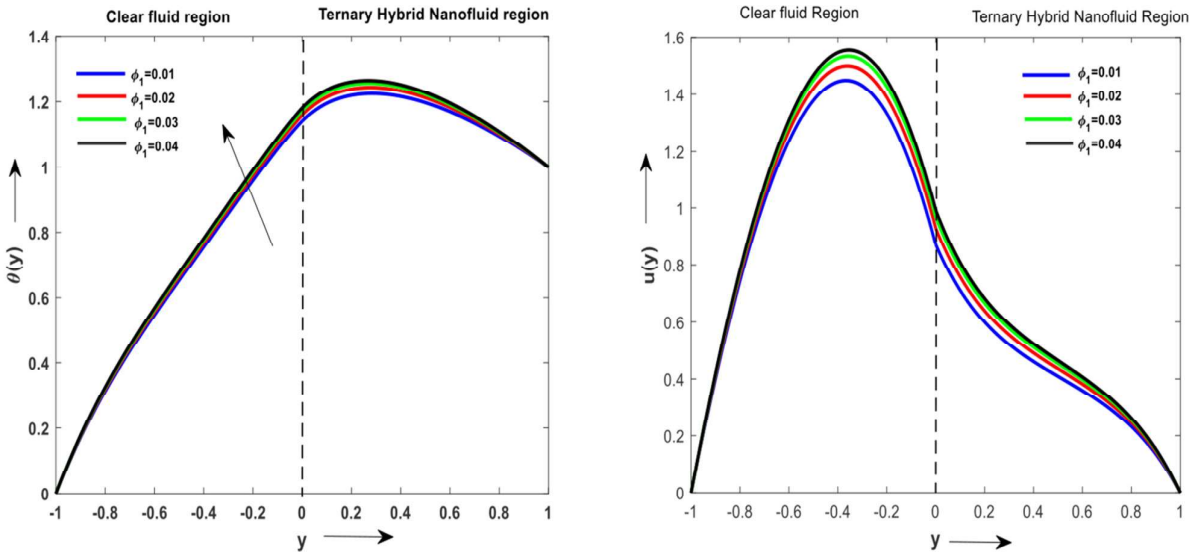

Figure 6. The impact of ϕ_1 on $\theta(y)$ and $u(y)$.

The effects of MgO and SWCNT volume fractions on temperature and velocity are illustrated in Figures 7 and 8. The value of the volume fractions of other nanoparticles is kept constant except for varying ones. In Figure 7, respectively, the effects of ϕ_2 on temperature and velocity are shown. As the solution's MgO concentration rises, the temperature falls. This is because of the material property of MgO, which reduces the fluid's temperature. As shown in Figure 7, the fluid's velocity decreases as the volume fraction of MgO increases. The fluid's temperature and velocity are affected by increasing the volume fraction of SWCNTs, as seen in Figure 8. With escalating ϕ_3 levels, both show a diminishing nature. A possible surface area for heat transfer is provided by the inclusion of various nanoparticle morphologies into the base fluid. In contrast, it stabilises the nanofluid, raising the fluid's temperature. Because of the nature of the substance, a few nanoparticles may have a cooling effect.

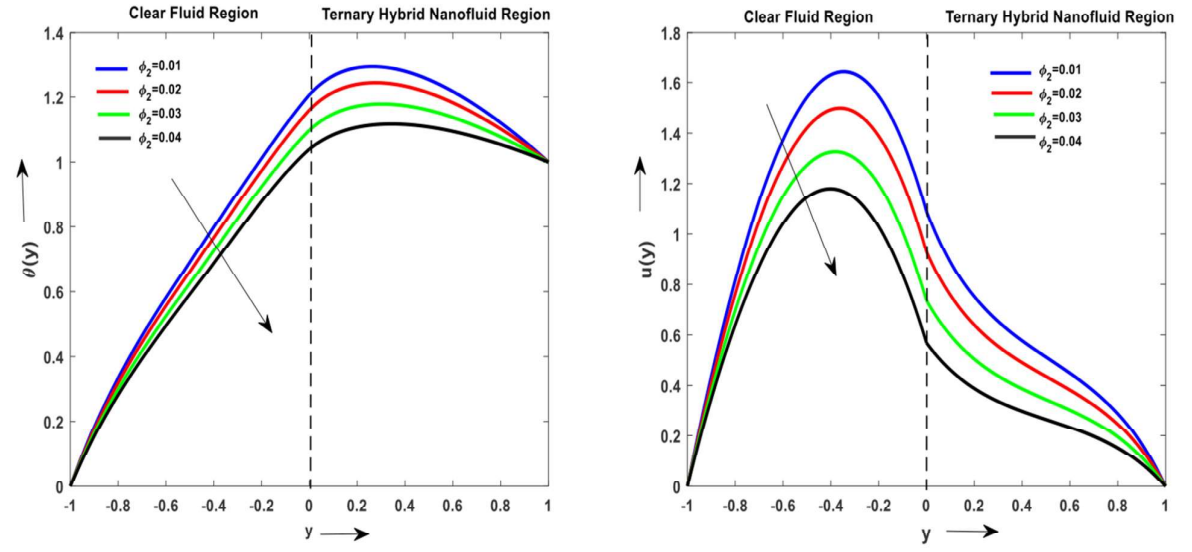

Figure 7. The impact of ϕ_2 on $\theta(y)$ and $u(y)$.

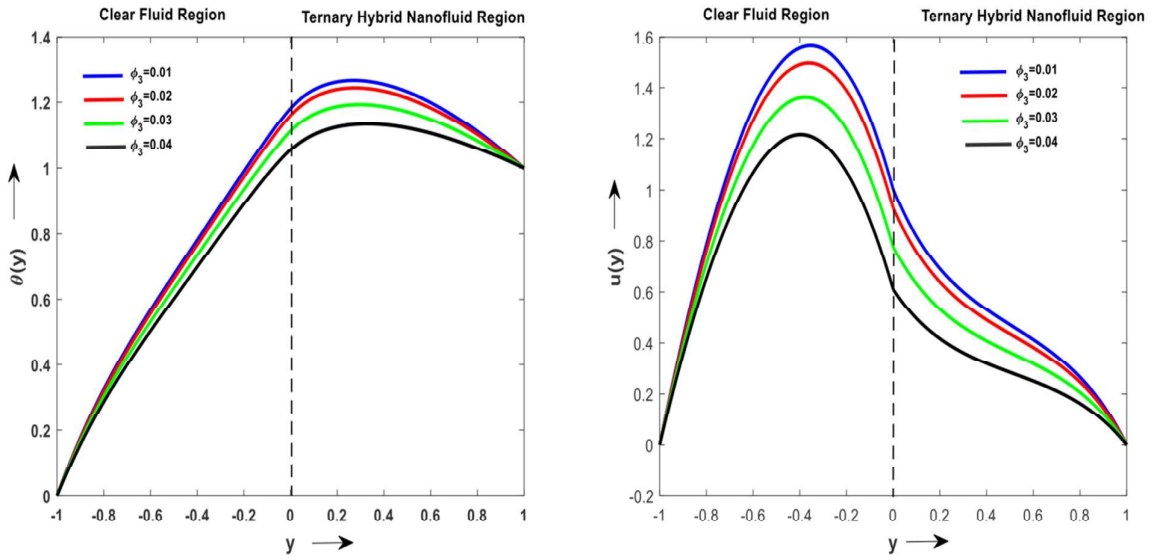

Figure 8. The impact of ϕ_3 on $\theta(y)$ and $u(y)$.

Figure 9 shows the impact of Grt and Br on Nu at both plates. According to Figure 9, Nu at $y = -1$ increases with Grt and Br. The colour transition in the graphs indicates that maximum Grt and Br values result in the highest heat transmission. Figure 9 illustrates how Grt and Br affect the Nusselt number at $y = 1$. Physically, rising levels of Grt and Br strengthen buoyancy and kinetic energy from viscous dissipation, strengthening convectional heat transmission. The fluid consequently acquires heat from the plate. The rate of heat transmission is considered to be at its maximum at $y = -1$.

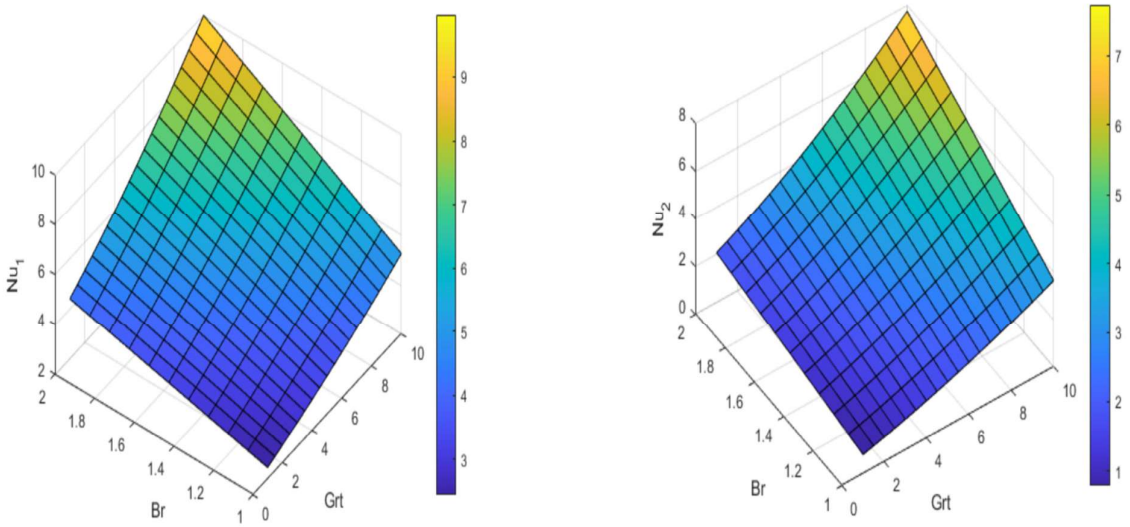

Figure 9. The effect of Grt and Br on Nusselt number at $y = -1$ and $y = 1$.

The effects of σ and R on Nu at both plates are depicted in Figure 10. Figure 10 in particular shows that as σ and R rise, Nu rises. On the other side, as permeability enhances, there is an increase in friction between the particles, which raises the temperature. In contrast, as R increases, the fluid's thermal conductivity decreases. These two elements have an impact on Nu. So, compared to Figure 9, Nu is lower.